

The variable stars in the field of the bulge cluster NGC 6558

A. Arellano Ferro,^{1*} L. J. Zerpa Guillen,^{2,3} M. A. Yepez,^{1,4} I. H. Bustos Fierro,⁵
Z. Prudil,⁶ C. E. Pérez Parra,^{2,3}

¹*Instituto de Astronomía, Universidad Nacional Autónoma de México, Ciudad de México, CP 04510, México.*

²*Universidad de Los Andes, Facultad de Ciencias, Dpto. Física, Grupo de Astrofísica Teórica, Mérida, Venezuela.*

³*Fundación Centro de Investigaciones de Astronomía Francisco, J. Duarte (CIDA), Mérida, Venezuela.*

⁴*Instituto Nacional de Astrofísica, Óptica y Electrónica (INAOE), Luis Enrique Erro No.1, Tonantzintla, Pue., C.P. 72840, México*

⁵*Observatorio Astronómico, Universidad Nacional de Córdoba, Córdoba C.P. 5000, Argentina.*

⁶*European Southern Observatory, , Karl-Schwarzschild-Straße 2, 85748, Garching, Germany*

Accepted: ; Received: 2020 in original form 2020 July

ABSTRACT

We made a survey of the variable stars in a 13.2×13.2 arcmin² centered on the field of the Galactic bulge cluster NGC 6558. A total of 78 variables was found in the field of the cluster. Many of these variables are included in the Catalogue of Variable Stars in Galactic Globular Clusters (Clement et al. 2001), OGLE or *Gaia*-DR3 data releases. A membership analysis based on the proper motions of *Gaia*-DR3 revealed that many of these variables do not belong to the cluster. We employed the data from the aforementioned surveys and our own data in the *VI* photometric system to estimate the periods, which along with the light curves morphology and position in a differentially dereddened colour- magnitude diagram (CMD), help classifying the variable types. Two new member variables were found; an eclipsing binary (V18) and a semi-regular SR/L (V19). In the end we conclude that only 9 variables are likely cluster members. Member variables were used to discuss the mean metallicity and distance of the parental cluster and find the average values .

Key words: globular clusters: individual (NGC 6558) – Horizontal branch – RR Lyrae stars – Fundamental parameters.

1 INTRODUCTION

The globular cluster NGC 6558 resides in the bulge of the Galaxy, very near to the Galactic center (Bica et al. 2016). From high resolution spectroscopic analysis of four red giants in NGC 6558 Barbuy et al. (2018) concluded that the cluster shows abundance pattern typical of the oldest inner bulge clusters and could be among the oldest objects in the Galaxy. Dynamically, the orbit of NGC 6558 is confined to less than 1.5 kpc (see the orbital integration in Fundamental parameters of Galactic globular cluster by Baumgardt et al. (2023)¹ from the Galactic center, confirming the cluster is a local resident with all rights.

Being the bulge regions very rich in stars and dust, the images of bulge clusters are highly contaminated with field stars and are generally subject to heavy interstellar differential reddening. Hence, to properly study the colour magnitude Diagram (CMD) of a bulge cluster, its stellar populations or families of variable stars, or to use specific groups of stars as indicators of physical properties, requires a thorough membership analysis and the calculation of a

reddening map across the field of the system (e.g. Alonso-García et al. (2012); Yepez et al. (2023)). Once this is achieved, then some of the variable stars can be used as indicators of cluster metallicity and distance, and their positions in the CMD can be compared with theoretical calculations to inferred evolutionary stages and internal stellar structure, in particular for the stars in the horizontal branch (HB). Previous studies carried out by our team towards the estimation of the main physical parameters; reddening, distance and metallicity employing their variable star populations are described in detail in the works by Arellano Ferro (2022) and Arellano Ferro (2024). The results for the bulge clusters NGC 6333, NGC 6401 and NGC 6522 are reported in the papers by Arellano Ferro et al. (2013), Tsapras et al. (2017) and Arellano Ferro et al. (2023) respectively.

2 OBSERVATIONS AND DATA REDUCTION

2.1 Bosque Alegre and Las Campanas Data

The data for this work were obtained with the 1.54 m telescope of the Bosque Alegre Astronomical Station (EABA), of the National Observatory of Córdoba, Argentina, during August-September 2018 and between June and August 2019, for a total of eleven nights. Two

* Corresponding Author: E-mail: armando@astro.unam.mx

¹ <https://people.smp.uq.edu.au/HolgerBaumgardt/globular/>

Table 1. Log of the observation of NGC 6558*.

Date	Site	N_V	t_V (s) sec	N_I	t_I (s) sec	Avg. seeing (")
2018-06-27	SWOPE	143	4 - 60	138	2 - 10	1.05
2018-06-29	SWOPE	101	4 - 80	98	2 - 10	1.37
2018-06-30	SWOPE	47	10 - 80	41	5 - 10	1.48
2018-08-04	EABA	44	120 - 200	39	100 - 60	2.65
2018-08-06	EABA	48	120	51	60	2.61
2018-08-12	EABA	39	120	39	60	3.38
2018-09-03	EABA	32	120	35	60	2.31
2018-09-15	EABA	21	120	27	60	2.38
2018-09-17	EABA	33	120	33	60	2.70
2019-06-29	EABA	43	120	53	60	3.19
2019-07-27	EABA	28	120	33	60	2.22
2019-07-28	EABA	54	120	51	60	2.44
2019-08-03	EABA	34	120	41	60	2.39
2019-08-10	EABA	51	120	52	60	2.95
Total:		718		731		

* Columns N_V and N_I record the number of images acquired while t_V , t_I indicate the typical exposure times. The average nightly seeing is given in the last column.

detectors were employed; in 2018 a CCD KAF-16803 with 4096×4096 pixels, while in 2019 a CCD KAF-6303E with 3072×2048 pixels. The corresponding fields were 16.9×16.9 arcmin² and 12.6×8.4 arcmin² respectively. Also observations were performed with the 1m telescope SWOPE from Las Campanas Observatory, Chile, during three nights in June 2018. The detector was a CCD E2V 231-81 with 4096×4112 pixels and a field of 14.8×14.9 arcmin². See Table 1 for the log of the observations. In the following we shall refer to EABA seasons as BA18 and BA19, and to Las Campanas seasons as SWOPE.

2.2 Data Reduction

To extract high-precision time-series photometry for all point sources in the field of our images, we employed the Difference Image Analysis (DIA) and the pipeline DanDIA (Bramich 2008); (Bramich et al. 2013); (Bramich et al. 2015).. The reference V and I images are obtained by stacking up images of the best quality in the collection. Then, individual images are subtracted from the reference to create individual differential images where the flux of all detected point sources is measured. The total flux in ADU/s is calculated as:

$$f_{\text{tot}}(t) = f_{\text{ref}} + \frac{f_{\text{diff}}(t)}{p(t)}, \quad (1)$$

where f_{ref} is the reference flux (ADU/s), $f_{\text{diff}}(t)$ the differential flux (ADU/s) and $p(t)$ is the photometric scale factor. To convert fluxes to instrumental magnitudes we used:

$$m_{\text{ins}}(t) = 25.0 - 2.5 \log[f_{\text{tot}}(t)], \quad (2)$$

where $m_{\text{ins}}(t)$ is the instrumental magnitude of the star at time t .

2.3 OGLE and Gaia-DR3 photometric data

We have also extensively used data of the variable stars in the field of the cluster identified in the OGLE and Gaia-DR3 data bases, and shall be discussed in the following sections.

Table 2. Season coefficients in transformation equation of the form $V - v = A(v - i) + B$, and $I - i = C(v - i) + D$.

Coeff.	SWOPE	EABA 2018	EABA 2019
A	-1.724 ± 0.0194	-2.726 ± 0.093	-3.19804 ± 0.04664
B	-0.101 ± 0.016	0.113 ± 0.139	0.15109 ± 0.05390
C	-4.172 ± 0.855	-3.589 ± 0.101	-3.94014 ± 0.04784

Table 3. Time-series VI photometry for the variables stars observed in this work*

Variable Star ID	Filter	HJD (d)	M_{std} (mag)	m_{ins} (mag)	σ_m (mag)
V1	V	2458342.52058	11.849	14.402	0.001
V1	V	2458342.52211	11.849	14.402	0.001
:	:	:	:	:	:
:	:	:	:	:	:
V1	I	2458342.51828	10.260	13.681	0.001
V1	I	2458342.51870	10.256	13.677	0.001
:	:	:	:	:	:
:	:	:	:	:	:
V3	V	2458727.54934	12.591	15.755	0.002
V3	V	2458727.55030	12.591	15.755	0.001
:	:	:	:	:	:
:	:	:	:	:	:
V3	I	2458727.54759	11.381	14.984	0.002
V3	I	2458727.54809	11.387	14.991	0.001
:	:	:	:	:	:
:	:	:	:	:	:

* The standard and instrumental magnitudes are listed in columns 4 and 5, respectively, corresponding to the variable stars in column 1. Filter and epoch of mid-exposure are listed in columns 2 and 3, respectively. The uncertainty on m_{ins} , which also corresponds to the uncertainty on M_{std} , is listed in column 6. A full version of this table is available at the CDS database.

2.4 Transformation to the VI standard system

The instrumental light curves can be converted into the standard system employing local standard stars in the field of the cluster. We found 9, 10 and 12 standard stars for the images in the seasons SWOPE, EABA2018 and EABA2019 respectively, in the catalogue of (Stetson 2000)², which have been set into the Johnson-Kron-Cousins standard system using the equatorial standards from Landolt (1992). The transformation equations are of the form $V - v = A(v - i) + B$, and $I - i = C(v - i) + D$, and the season constants are reported in Table 2.

In Table 3 we include a small portion of the time-series VI photometry obtained in this work. The full table shall be available in electronic form in the Centre de Donnés astronomiques de Strasbourg database (CDS).

3 MEMBERSHIP ANALYSIS

Being in the Galactic bulge, the colour-magnitude diagram (CMD) of NGC 6558 is heavily contaminated by field stars all subject to a remarkable differential reddening. To produce a clean and useful CMD a membership analysis and a local reddening map are in order.

The membership analysis was performed using the positions and proper motions available in the Gaia-DR3 and employing the method of Bustos Fierro & Calderón (2019). The method is based on a two step approach: 1) it finds groups of stars with similar characteristics in the four-dimensional space of the gnomonic coordinates (X_t, Y_t) and proper motions $(\mu_{\alpha^*}, \mu_{\delta})$ employing the BIRCH

² <https://www.canfar.net/storage/list/STETSON/Standards>

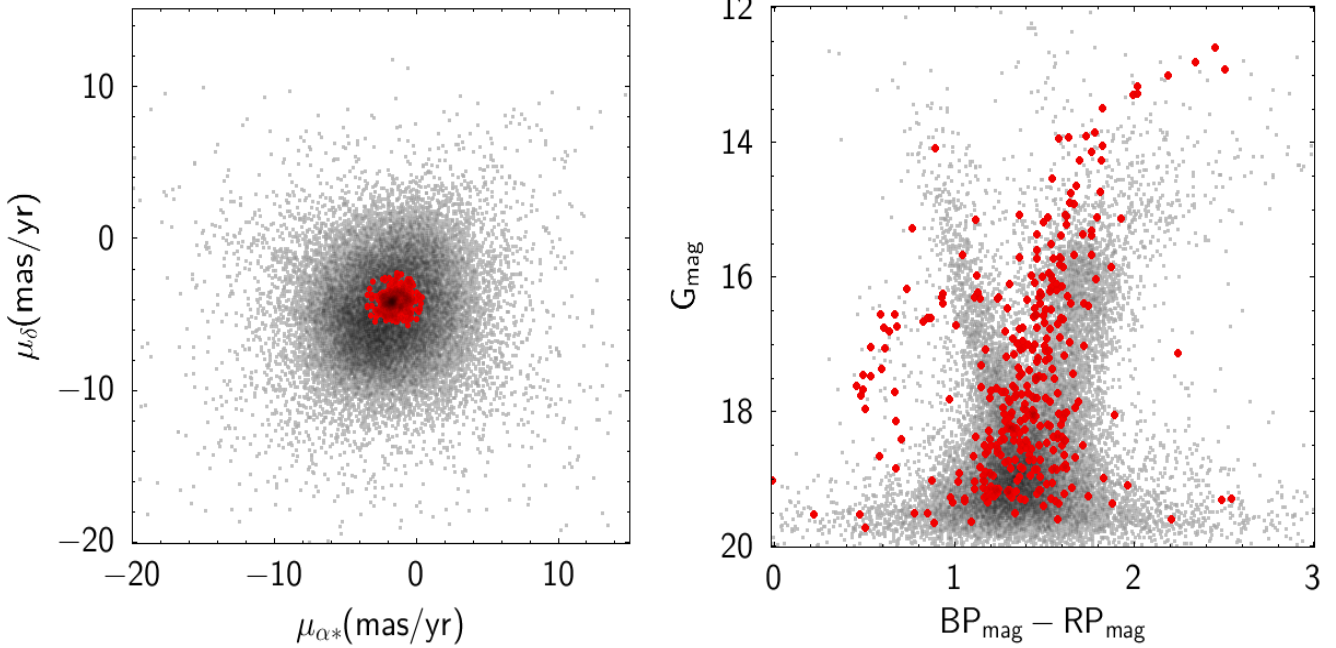


Figure 1. Results from the membership analysis (section 3). Left and right panels show the vector point (VPD) and CMD diagrams respectively. Red dots represent the likely cluster members while the gray dots represent the field stars.

clustering algorithm (Zhang et al. 1996) and 2) in order to extract likely members that were missed in the first stage, the analysis of the projected distribution of stars with different proper motions around the mean proper motion of the cluster is performed.

There are 45,506 point sources within an 8 arcmin field centered in the cluster. However, proper motions are available for only 28,334. Most of the stars were found field stars and only 495 were identified as likely cluster members. Fig. 1 displays the results in the Vector-Point diagram (VPD) and the resulting Colour-Magnitude diagram (CMD). The identified likely members clearly trace the major features in the CMD, such as the horizontal branch (HB) and the red giant branch (RGB).

4 DIFFERENTIAL REDDENING AND THE CMD

To properly deredden the colour magnitude diagram of this bulge cluster, it is necessary to consider the effects of differential reddening. Fortunately, NGC 6558 has been included in the thorough reddening study of the inner Galaxy by Alonso-García et al. (2012). We used their reddening map to differentially deredden the VI CMD obtained from our photometry.

In Fig. 2 we display on the left panel the CMD dereddened with a constant value $E(B-V) = 0.40$. On the right panel we have applied the differential corrections guided by the reddening map, i.e. $E(B-V) + diff$, where $diff$ corresponds to the differential corrections for the corresponding position of the star. The improvement on the dispersion at the RGB and the HB are obvious

5 THE VARIABLE STARS IN NGC 6558

The field of NGC 6558, like in most of the bulge clusters, is very rich in variable stars. The advent of missions like *Gaia* and OGLE have detected a large number of them. However, many of these variables

are not linked to the cluster but are merely projected against it. Our aim in the following sections is to critically evaluate the membership of them. The challenge is to achieve good photometric values that entitle us to position the variables in our observed and properly dereddened VI CMD, which along with the proper motion analysis, their pulsational type and, in the case of RR Lyrae, the estimation of their distance via the Fourier decomposition of their light curves, should allow us to pronounce about their membership status.

5.1 The catalogued variables (Clement et al. 2001)

The catalogue of variable stars in globular clusters (CVSGC) (Clement et al. 2001) in its April 2016 update, lists 17 variables and labels two of them (V2 and V7) as probably non-variable. The rest are 8 RRab, 3 RRc, and 4 long period variables labeled "L?"

5.2 Other variables in the field of NGC 6558 according to OGLE, and *Gaia*

In the *Gaia* mission (Gaia Collaboration et al. 2016) and the Optical Gravitational Lensing Experiment (OGLE) (Udalski et al. 1992) many variables were detected in the field of NGC 6558. We have cross-matched those variables with point sources measured in our photometry and have combined the photometric data to build the light curves. In the case of OGLE III (Soszyński et al. 2013) and IV (Soszyński et al. 2014), VI magnitudes are available. For the case of *Gaia*-DR3 data, a transformation into the VI system was necessary. This was achieved using the transformation equations of (Riello et al. 2021).

We identified 56 variables in the OGLE data base within the field of NGC 6558 and for the present purpose of the paper we shall identify them with the prefix 'O'. Similarly we noticed 13 stars announced as variable in *Gaia*-DR3, these stars we call them with the prefix 'G'. Then we aim to confirm their variability and type, and

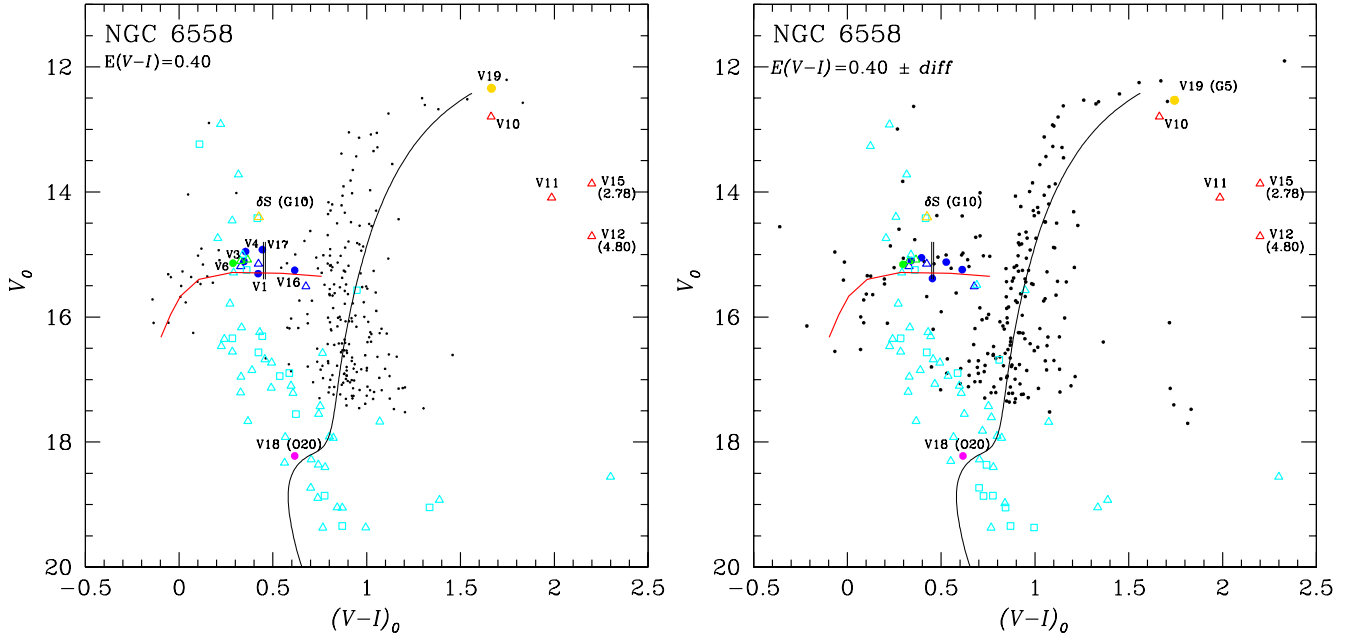


Figure 2. The CMDs built from cluster members measured by our VI photometry. The panel on the left shows the CMD dereddened with an average $E(B - V) = 0.40$ while the one to the right has been differentially dereddened as described in section 4. The improvement after the corrections is clear. Variable stars in the field of the cluster, members and no members, are shown by colour symbols according to the following code: RRab-blue; RRC-green; RGB-red; δ Sct (G10) and member RGB (V19) -yellow; binaries -turquoise; member binary V18 (O20)-magenta. Solid symbols are used for members and empty ones for field stars (triangles) or stars of unknown status due to lack of proper motion (squares). The isochrone is from [VandenBerg et al. \(2014\)](#) for $[\text{Fe}/\text{H}] = -1.35$ and an age of 12.0 Gyrs. Red ZAHB is from the models built from the Eggleton code ([Pols et al. 1997, 1998](#); [Schroder et al. 1997](#)), and calculated by [Yepez et al. \(2022\)](#). The vertical black lines at the ZAHB mark the empirical red edge of the first overtone instability strip ([Arellano Ferro et al. 2015, 2016](#)).

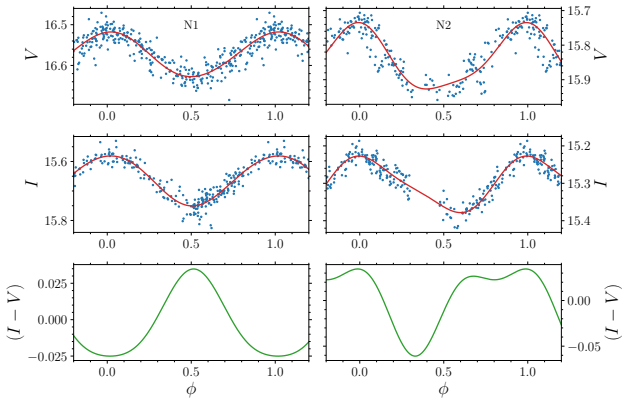


Figure 3. Two newly detected variables, N1 and N2, which do not pertain to NGC 6558. Their light curves are phased with periods 0.303797 d and 0.342412 d respectively. Blue points represent observations, Fourier fits to observed data are marked in red, and green lines (bottom panel) stand for the difference between Fourier fits to illustrate colour variation.

to check their membership. The table cross matching the variables in the CVSGC, OGLE and *Gaia*, indicating their membership status, and their light curves are reported in Appendix A at the end of the paper.

In the process we discovered two variables not reported neither in *Gaia* nor in OGLE databases and which we identified as N1 and N2. In our membership analysis these stars were found to be field stars. Their light curves are shown in Fig. 3. Judging by their periods and light curve morphology they resemble RRC variables,

however we note that for N1 the amplitude in the I -band is a bit larger than in the V -band ($\text{Amp}_V = 0.110 \pm 0.002$ mag and $\text{Amp}_I = 0.170 \pm 0.003$ mag), which is unusual. On the other hand, N2 exhibits expected amplitude difference with amplitude in the V -band being larger ($\text{Amp}_V = 0.193 \pm 0.005$ mag and $\text{Amp}_I = 0.151 \pm 0.003$ mag).

In the identification chart of Fig. 4 we include all stars listed in the CVSGC (2016 edition) plus the two new member variables discovered in this work (V18 and V19). Note that V2 and V7 in fact do not show signs of variability, and that 10 of them are not cluster members, as indicated in Table A1.

6 THE COLOUR-MAGNITUDE DIAGRAM

In the CMD of Fig. 2 we included all the variables in the field of NGC 6558 coded as described in the caption. All stars whose variability has been confirmed are plotted using their intensity-weighted means $\langle V \rangle_0$ and corresponding colour $\langle V \rangle_0 - \langle I \rangle_0$. Filled and empty symbols were used for members and either field stars or of unknown status due to the lack of proper motions in the *Gaia*-DR3 database.

All member variables occupy the expected regions according to their variable type. We note the distribution of RRab stars relative to the empirical first overtone red edge (FORE) indicated in the DCM by the vertical black lines in the HB. See Fig. 5 for an expanded version of the HB region. There is evidence that at least two RRab stars V3 and V4, are sitting to the left of the FORE, i.e. in the bimodal or "either-or" region, shared by fundamental and first overtone mode pulsators. Both stars show signs of amplitude modulations. The period analysis of V4 (RRLYR-14866) using *Period04* ([Lenz &](#)

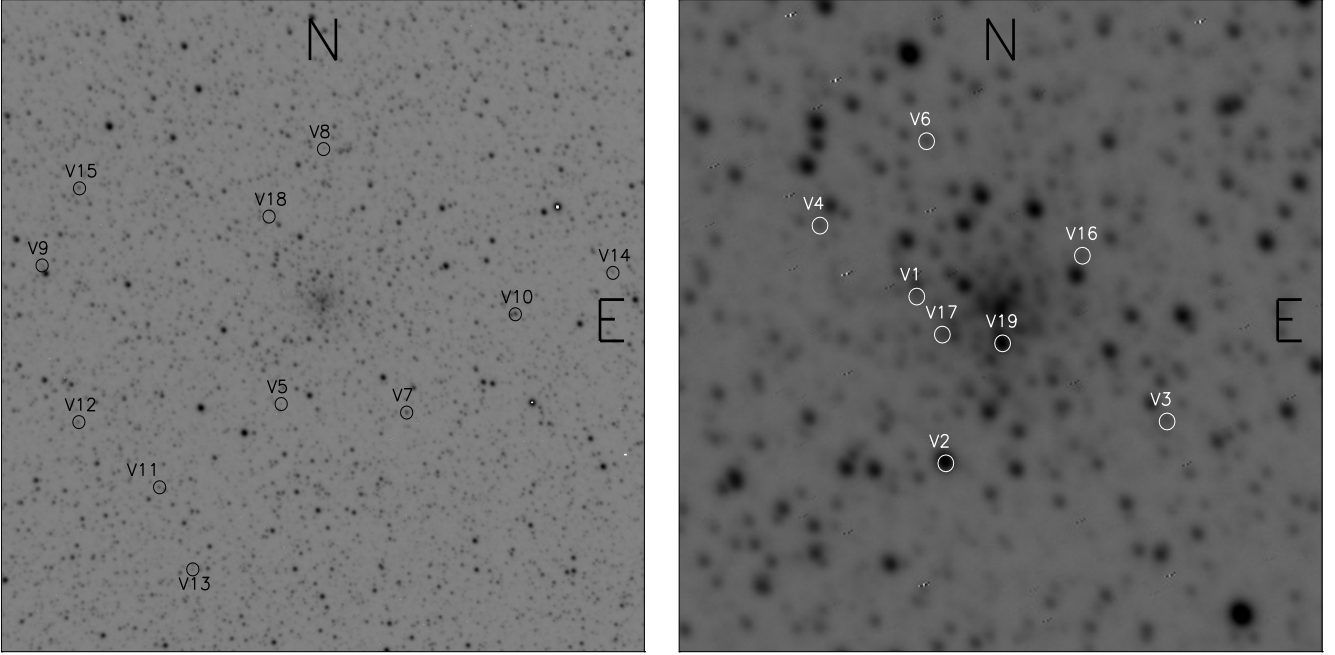


Figure 4. Identification chart of the cluster member variable stars NGC 6558. The field of the left panel is about 13.2×13.2 arcmin² whereas the central region in the right panel is approximately 3.3×3.3 arcmin²

Table 4. Fourier coefficients for RRab stars. The numbers in parentheses indicate the uncertainty on the last decimal place. The deviation parameter D_m is given in the last column.

Variable	A_0 (V mag)	A_1 (V mag)	A_2 (V mag)	A_3 (V mag)	A_4 (V mag)	ϕ_{21}	ϕ_{31}	ϕ_{41}	D_m
V1	16.634(2)	0.382(2)	0.177(2)	0.124(2)	0.077(2)	3.8453(19)	8.127(27)	6.133(41)	2.7
V3	16.280(3)	0.456(4)	0.239(4)	0.133(4)	0.103(4)	4.013(23)	8.279(38)	6.487(48)	4.3
V4	16.439(4)	0.405(4)	0.198(3)	0.140(3)	0.086(3)	3.944(21)	8.159(31)	6.174(46)	1.1
V16	16.579(1)	0.128(2)	0.052(2)	0.007(2)	0.006(2)	4.497(35)	9.557(187)	7.813(296)	3.7
V17	16.248(1)	0.093(1)	0.019(1)	0.005(1)	0.001(1)	4.508(82)	9.116(28)	8.049(99)	5.2

Table 5. Physical parameters for the RRab stars. The numbers in parentheses indicate the uncertainty on the last decimal place.

Variable	[Fe/H] _{ZW}	[Fe/H] _{UVES}	[Fe/H] _{DK†}	M_V	$\log T_{\text{eff}}$	$\log (L/L_{\odot})$	D (kpc)	M/M_{\odot}	R/R_{\odot}
V1	-1.21(3)	-1.09(3)	-1.309	0.691(3)	3.822(8)	1.626(1)	9.01(1)	0.70(7)	4.49(1)
V3	-1.52(4)	-1.44(4)	-1.994*	0.423(6)	3.810(9)	1.741(2)	8.75(3)	0.79(8)	5.56(2)
V4	-1.32(3)	-1.20(3)	-1.296	0.614(4)	3.818(9)	1.659(2)	8.21(3)	0.71(7)	4.69(1)
V16	-0.70(22)*	-0.68(12)*	-1.240	0.573(3)	3.807(34)	1.663(1)	8.98(1)	0.52(21)	5.63(10)
V17	-1.37(5)	-1.26(5)	-1.257	0.535(1)	3.786(13)	1.692(1)	7.84(3)	0.63(10)	5.94(2)
Weighted Mean	-1.33(2)	-1.20(2)	-1.280	0.569(8)	3.813(1)	1.670(1)	8.47(4)	0.69(3)	5.66(2)
σ	± 0.11	± 0.13	± 0.028	± 0.089	± 0.012	± 0.039	± 0.46	± 0.09	± 0.57

† Iron values from Dékány et al. (2021). The extreme value of V3 is likely due to blending and was not averaged. *Not included in the average of [Fe/H] due to uncertain ϕ_{31} .

Breger 2004) shows a periodic modulation of the light curve equal to $P_{\text{BL}} = 26.73 \pm 0.01$ day (known as the Blazhko effect, Blažko 1907). V1, fundamental mode variable, seems a border case between blue and red parts of the instability strip.

According to Arellano Ferro et al. (2019) (their figure 8) or Deras et al. (2022) (their figure 7), the presence of fundamental mode RRab stars in the bimodal region is an exclusive characteristic of some Oo I clusters, and does not occur in Oo II type clusters.

This comment is of relevance considering that the Oosterhoff type of NGC 6558 cannot be assessed clearly: in the Bailey's diagram of Fig. 6 member stars are few and their distribution do not decant in favour of either Oo I or OoII sequences; the average period of the 5 member RRab stars is 0.60 ± 0.04 day which is the border between Oosterhoff types. The empirical border $[\text{Fe}/\text{H}]_{\text{ZW}} \sim -1.5$ between the metal poor Oo II and the metal richer Oo I (Arellano Ferro 2024), and the value of $[\text{Fe}/\text{H}]_{\text{ZW}} = -1.33 \pm 0.11$ obtained

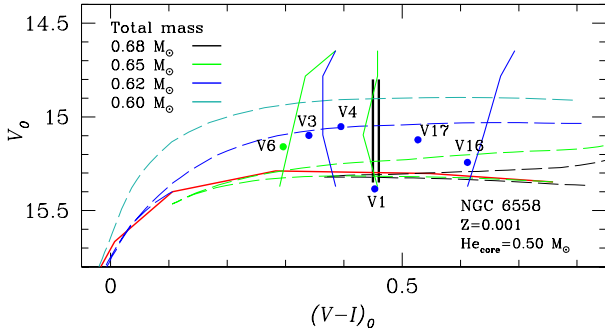


Figure 5. Horizontal branch region of NGC 6558. Blue and green symbols represent RRab and RRc cluster member stars respectively. Red continuous line and vertical black lines are the ZAHB and first overtone red edge described in the caption of Fig. 2. Segmented lines are evolutionary tracks with total and core masses given in the figure legend. Blue and green vertical loci represent the instability strip borders for the fundamental and first overtone respectively (Bono et al. 1994)

. See Section 9 for a discussion.

from the Fourier decomposition of the best observed members (V1, V3, V4 and V17). The above average period and metallicity, when plotted on the plane $[\text{Fe}/\text{H}]$ vs $\langle P_{ab} \rangle$ of figure 5 of Catelan (2009), places the cluster in the Oosterhoff gap, suggesting that NGC 6558 is of the intermediate Oosterhoff type or Oo-Int. We note that in the work by Catelan (2009), NGC 6558 was classified as Oo I due to the lower average pulsation period for associated fundamental mode pulsators.

A revision of the membership probabilities assigned by Vasiliev & Baumgardt (2021) for stars in the field of NGC 6558, confirm the membership status of V3, V16 and V17, but assigns very low probabilities to V1 and V4. If these two stars are not considered members the average $\langle P_{ab} \rangle$ becomes 0.677 d, which would only highlight NGC 6558 as a peculiar cluster in the $[\text{Fe}/\text{H}]$ vs $\langle P_{ab} \rangle$ plane, i.e. too high a metallicity for its average period. Two clusters with a similar property are the moderate metal-rich Oo III clusters NGC 6388 and NGC 6441 which, in spite their extended HB blue tails (Piotto et al. 1997; Rich et al. 1997), they display a prominent red-clump which is absent in NGC 6558.

In our opinion and based on our membership analysis, the five RRab members lead to a value of $\langle P_{ab} \rangle = 0.60 \pm 0.04$, which puts the cluster in the Oosterhoff gap in the $[\text{Fe}/\text{H}]$ vs $\langle P_{ab} \rangle$ plane and NGC 6558 should be considered of an Oo-int nature.

7 FOURIER LIGHT CURVE DECOMPOSITION OF MEMBER RR LYRAE

We identified five RRab member stars of the cluster. In this section we perform a Fourier decomposition of their light curves and use their Fourier parameters and ad-hoc semi-empirical calibrations to estimate their metallicity and distance. For brevity we will not repeat here the description of this approach since it has been thoroughly described by Arellano Ferro et al. (2010) and summarized by Arellano Ferro (2024).

In Table 4 the Fourier coefficients of the five member RRab are listed as it is their consistency parameter D_m defined by (Jurcsik & Kovács 1996). According to these authors, the $[\text{Fe}/\text{H}]$ calibration for RRab stars is applicable for values of $D_m < 3.0$. We have relaxed this criterion a bit to $D_m < 5.0$ to increase the possibilities of our sample.

We recall that the iron abundance value obtained photometrically from this calibration is given into the scale of Jurcsik and Kovács, $[\text{Fe}/\text{H}]_{\text{JK}}$, which can be converted into the scale of Zinn & West (1984) via $[\text{Fe}/\text{H}]_{\text{JK}} = 1.431[\text{Fe}/\text{H}]_{\text{ZW}} + 0.88$ (Jurcsik & Kovács 1996) and in turn it can be transformed into the spectroscopic scale of Carretta et al. (2009) via $[\text{Fe}/\text{H}]_{\text{UVES}} = -0.413 + 0.130[\text{Fe}/\text{H}]_{\text{ZW}} - 0.356[\text{Fe}/\text{H}]_{\text{ZW}}^2$. In Table 5 we report the mean physical parameter obtained for the 5 RRab stars. For comparison, we have included in column 4 of Tab. 5 the iron values estimated by Dékány et al. (2021) $[\text{Fe}/\text{H}]_{\text{DK}}$, for the same RR Lyrae in NGC 6558. These authors used the photometric Fourier decomposition approach considering newly calculated calibrations of the I -band light curve parameters. The average $[\text{Fe}/\text{H}]_{\text{DK}}$ matches well our results for $[\text{Fe}/\text{H}]_{\text{UVES}}$.

8 ON THE DISTANCE TO NGC 6558

The P-L (I) calibration for RR Lyrae stars can be used to produce independent estimates of the distance. We have employed two calibrations available in the literature. Catelan et al. (2004) calculated the equation $M_I = 0.471 - 1.132 \log P + 0.205 \log Z$, with $\log Z = [M/H] - 1.765$; $[M/H] = [\text{Fe}/\text{H}] - \log(0.638 f + 0.362)$ and $\log f = [\alpha/\text{Fe}]$, from where we adopted $[\alpha/\text{Fe}] = +0.4$ (Salaris et al. 1993). For the calculation, we have adopted the value of the metallicity $[\text{Fe}/\text{H}]_{\text{UV}} = -1.20$, obtained from the Fourier approach (see Table 5, and the average $E(B-V) = 0.40$. We applied the above calibration to the five RRab stars in Table 5 and the RRc star V6. The period of the latter was fundamentalized using the ratio $P_1/P_0 = 0.75$. The resulting mean distance was 8.10 ± 0.22 kpc, which is in good agreement with the result from the Fourier approach of 8.47 ± 0.46 kpc.

On the other hand, a recent P-L (I) calibration calculated by Prudil et al. (2024) using data published by the *Gaia*-DR3 is of the form $M_I = 0.197 - 1.292 \log P + 0.196 [\text{Fe}/\text{H}]$. When this equation is applied to the six cluster members RRab and RRc, a mean distance of 7.72 ± 0.20 kpc was found. We note that for the treatment of reddening and differential reddening, we used reddening maps and laws from Schlegel et al. (1998) and Alonso-García et al. (2012, see Section 4).

With the P-L relations in the aforementioned paper, Prudil et al. (2024) derived reddening maps and reddening laws for the following four colours: $(J - K_s)$, $(I - K_s)$, $(V - I)$ and $(G_{\text{BP}} - I)$. Using the newly reddening maps and reddening laws, solely based on individual RR Lyrae variables toward the Galactic bulge, we have obtained their distances, using a similar approach as used by Prudil et al. (2019). The results are shown in Table 7. In the last column, we have averaged the results for colours $(J - K_s)$ and $(V - I)$ which in turn lead to a grand average of 8.73 ± 0.29 . Comparing these results with those in Table 6 we point to the agreement, within the respective uncertainties, with the distance obtained from the Fourier light curve decomposition approach.

It should be noted that in their compilation of globular cluster distances, Baumgardt et al. 2023³ the distances determined for NGC 6558 prior to 1998, tend to be smaller than 8 kpc and the authors report an average of 7.79 ± 0.18 kpc. In their paper Baumgardt & Vasiliev (2021) the reported mean distance is 7.47 ± 0.29 kpc. In either case our calculations via the Fourier approach and the P-L(I) relationship render a distance a bit larger than 8 kpc, as stated

³ <https://people.smp.uq.edu.au/HolgerBaumgardt/globular/>

Table 6. Summary of distance estimates of NGC 6558.

D kpc	source
8.47 ± 0.46	This work RR Lyrae Fourier decomposition
8.10 ± 0.22	P-1 (I) (Catelan et al. 2004)
7.72 ± 0.20	P-1 (I) (Prudil et al. 2024)
7.79 ± 0.18	Baumgardt et al. (2023) compilation
7.47 ± 0.29	(Baumgardt & Vasiliev 2021)

above. For a clearer reference, in Table 6 we summarize all the above distances and methods

9 MODELLING THE HORIZONTAL BRANCH

There is a clear correlation between the HB extension to the blue and the metallicity among globular clusters (Sandage & Wallerstein 1960); the lower the metallicity, the bluer the HB. The temperature of a HB star depends both on the metallicity (lower metallicity produces lesser opacities and then more compact, hotter, and bluer shells), but also on the mass of a H-rich shell. It was noted by Schröder & Cuntz (2005) that by comparing models of a given metallicity but different shell masses it can be shown that lower shell masses also produce bluer HB stars.

The role of mass loss during the He-flashes events at the RGB upon the colour of a He-core burning star settling on the HB, has been illustrated by Silva Aguirre et al. (2008). The more mass is lost in the RGB the bluer the star will be on the ZAHB when the helium core gets ignited.

To model the RR Lyrae region of NGC 6558 we used the code employed by Schröder & Cuntz (2005) that uses a modified Reimers law with $\eta = 0.8 \times 10^{-13}$. This original evolution code developed by Eggleton (1971, 1972, 1973) and further improved and thoroughly tested by Pols et al. (1997, 1998) and Schroder et al. (1997). We here use abundances for $Z=0.001$, equivalent to $[\text{Fe}/\text{H}] = -1.3$ dex, similar to the metallicity found for NGC 6558.

In Fig. 5 the five cluster member RR Lyrae are shown on an expanded version of the HB region. The stars are well represented by models with a core mass of $0.50 M_{\odot}$ and a range of shell mass between 0.10 and $0.18 M_{\odot}$. The main-sequence progenitor of these stars is a 0.82 - $0.86 M_{\odot}$ star that reached the RGB after approximately 13 and 11 Gyrs respectively, where it lost some 20 to 30% of its mass before evolving to the ZAHB.

In older globular clusters, HB stars have developed from slightly lower mass stars on the main sequence. Since the degenerate Helium-core needs in all cases $\sim 0.5 M_{\odot}$ to start the central He-burning, then the resulting H-rich shell mass are smaller and bluer. We have argued (Arellano Ferro et al. 2020) that the range of colour on the HB population, larger than expected from a suitable model and their moves on the HRD (Vandenberg & Durrell 1990), can be explained by slight variations of the mass loss on the RGB, which produces certain shell-mass range of HB stars in the same globular cluster. A moderate star-to-star variation of mass-loss would make a simple explanation for the extended colour distributions on the HB. We have also speculated that mass-loss in the RGB may be modulated by the presence of magnetic fields in red giants (Konstantinova-Antova et al. 2013).

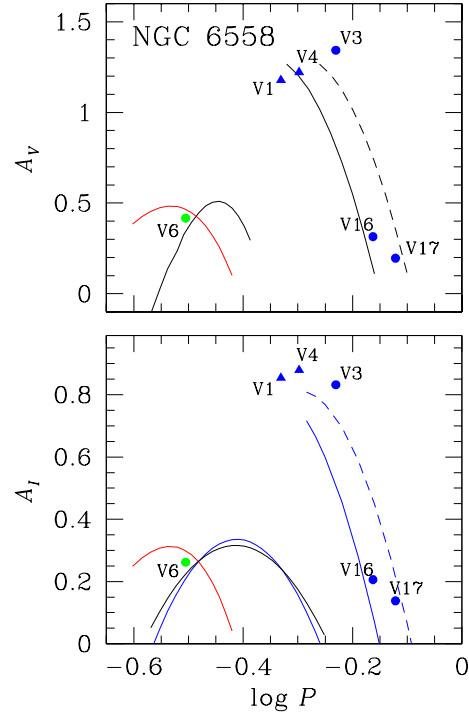


Figure 6. Period-Amplitude diagram. Continuous and segmented loci to the right are indications of Oo I and Oo II types respectively for the RRab stars distribution (Cacciari et al. 2005) and (Kunder et al. 2013a); likewise are the red and black parabolas for RRc stars (Kunder et al. 2013b) and (Yepez et al. 2020). The distribution of stars do not favour neither Oo I nor Oo II types. The RRab variables V1 and V4 were found to be cluster members in our analysis, but were given a low membership probability by the analysis of Vasiliev & Baumgardt (2021)

. See discussion in section 6.

10 SUMMARY AND CONCLUSIONS

Since the stellar field in the Galactic bulge is densely populated, the number of variable stars in the field of a Galactic bulge cluster can seem very large, however, it is very likely that many of those variables do not pertain to the cluster. That such is the case of NGC 6558 has been demonstrated in this work. In the Catalogue of Variable Stars in Galactic Globular Clusters, OGLE and *Gaia*-DR3 data, we identified 78 stars in the field of NGC 6558. However a proper motion analysis and a thorough exploration of this variables on the CMD of the cluster shows that only 9 of them seem to be truly cluster members.

We have then Fourier decomposed the light curves of the five RRab members to estimate the mean distance and metallicity of the cluster as 8.47 ± 0.46 kpc and $[\text{Fe}/\text{H}]_{\text{ZW}} = -1.33 \pm 0.11$, or in the spectroscopic scale of Carretta et al. (2009) $[\text{Fe}/\text{H}]_{\text{UVES}} = -1.20 \pm 0.13$.

A cross identification of all variables in the field of the cluster between their OGLE and *Gaia*-DR3 numbers is provided and *VI* light curves are displayed and made available in the Centre de Donnés astronomiques de Strasbourg database (CDS). Their ephemerides, AR and DEC, and mean *VI* magnitudes and amplitudes are also tabulated.

Acknowledgements. AAF is grateful to the Indian Institute of Astrophysics, and to the European Southern Observatroy for warm hospitality during the preparation of this work. AAF also thankfully acknowledges the sabbatical support granted by the program PASPA of the DGAPA-UNAM. We have been benefited from the support

Table 7. Cluster member RR Lyrae distances (derived in Prudil et al. 2024, submitted) based on P-L relations of Prudil et al. (2024).

ID Star	ID OGLE	D_{J-K_s} (kpc)	D_{I-K_s} (kpc)	D_{V-I} (kpc)	D_{GBP-I} (kpc)	Avg [$D_{J-K_s}; D_{V-I}$] (kpc)
V1	RRLYR-14886	7.73	7.68	8.77	9.40	8.25
V3	RRLYR-14929	9.00	8.93	8.87	7.22	8.94
V4	RRLYR-14866	9.24	9.28	9.00	8.57	9.12
V6	RRLYR-14888	8.77	8.89	8.61	8.14	8.83
V16	RRLYR-14912	8.86	8.85	8.10	7.93	8.48
V17	RRLYR-14892	9.01	9.02	8.53	8.49	8.77
Average						8.73±0.29

of DGAPA-UNAM through projects IG100620 and IN103024. We have made an extensive use of the SIMBAD and ADS services, for which we are thankful.

Data Availability: The data underlying this article shall be available in electronic form in the Centre de Données astronomiques de Strasbourg database (CDS), and can also be shared on request to the corresponding author.

REFERENCES

- Alonso-García J., Mateo M., Sen B., Banerjee M., Catelan M., Minniti D., von Braun K., 2012, *AJ*, **143**, 70
- Arellano Ferro A., 2022, *RevMexA&A*, **58**, 257
- Arellano Ferro A., 2024, *IAU Symposium*, **376**, 222
- Arellano Ferro A., Giridhar S., Bramich D. M., 2010, *MNRAS*, **402**, 226
- Arellano Ferro A., et al., 2013, *MNRAS*, **434**, 1220
- Arellano Ferro A., Mancera Piña P. E., Bramich D. M., Giridhar S., Ahumada J. A., Kains N., Kuppuswamy K., 2015, *MNRAS*, **452**, 727
- Arellano Ferro A., Luna A., Bramich D. M., Giridhar S., Ahumada J. A., Muneer S., 2016, *Ap&SS*, **361**, 175
- Arellano Ferro A., Bustos Fierro I. H., Calderón J. H., Ahumada J. A., 2019, *Rev. Mex. Astron. Astrofis.*, **55**, 337
- Arellano Ferro A., Yepez M. A., Muneer S., Bustos Fierro I. H., Schröder K. P., Giridhar S., Calderón J. H., 2020, *MNRAS*, **499**, 4026
- Arellano Ferro A., Prudil Z., Yepez M. A., Bustos Fierro I., Luna A., 2023, *Ap&SS*, **368**, 91
- Barbuy B., et al., 2018, *A&A*, **619**, A178
- Baumgardt H., Vasiliev E., 2021, *MNRAS*, **505**, 5957
- Bica E., Ortolani S., Barbuy B., 2016, *Publ. Astron. Soc. Australia*, **33**, e028
- Blažko S., 1907, *Astronomische Nachrichten*, **175**, 325
- Bono G., Caputo F., Stellingwerf R. F., 1994, *ApJ*, **423**, 294
- Bramich D. M., 2008, *MNRAS*, **386**, L77
- Bramich D. M., et al., 2013, *MNRAS*, **428**, 2275
- Bramich D. M., Bachelet E., Alsubai K. A., Mislis D., Parley N., 2015, *A&A*, **577**, A108
- Bustos Fierro I. H., Calderón J. H., 2019, *MNRAS*, **488**, 3024
- Cacciari C., Corwin T. M., Carney B. W., 2005, *AJ*, **129**, 267
- Carretta E., Bragaglia A., Gratton R., D’Orazi V., Lucatello S., 2009, *A&A*, **508**, 695
- Catelan M., 2009, *Ap&SS*, **320**, 261
- Catelan M., Pritzl B. J., Smith H. A., 2004, *ApJS*, **154**, 633
- Clement C. M., et al., 2001, *AJ*, **122**, 2587
- Dékány I., Grebel E. K., Pojmański G., 2021, *ApJ*, **920**, 33
- Deras D., Arellano Ferro A., Bustos Fierro I., Yepez M. A., 2022, *Rev. Mex. Astron. Astrofis.*, **58**, 121
- Eggleton P. P., 1971, *MNRAS*, **151**, 351
- Eggleton P. P., 1972, *MNRAS*, **156**, 361
- Eggleton P. P., 1973, *MNRAS*, **163**, 279
- Gaia Collaboration Prusti T., de Bruijne J. H. J., et al. 2016, *A&A*, **595**, A1
- Gaia Collaboration et al., 2018, *A&A*, **616**, A1
- Jurcsik J., Kovács G., 1996, *A&A*, **312**, 111
- Konstantinova-Antova R., et al., 2013, *Bulgarian Astronomical Journal*, **19**, 14
- Kunder A., Stetson P. B., Catelan M., Walker A. R., Amigo P., 2013a, *AJ*, **145**, 33
- Kunder A., et al., 2013b, *AJ*, **146**, 119
- Landolt A. U., 1992, *AJ*, **104**, 340
- Lenz P., Breger M., 2004, in Zverko J., Ziznovsky J., Adelman S. J., Weiss W. W., eds, *IAU Symposium Vol. 224, The A-Star Puzzle*. pp 786–790, doi:10.1017/S1743921305009750
- Piotto G., et al., 1997, in *Stellar Ecology: Advances in Stellar Evolution*, pp 84–91 (arXiv:astro-ph/9701152), doi:10.48550/arXiv.astro-ph/9701152
- Pols O. R., Tout C. A., Schroder K.-P., Eggleton P. P., Manners J., 1997, *MNRAS*, **289**, 869
- Pols O. R., Schröder K.-P., Hurley J. R., Tout C. A., Eggleton P. P., 1998, *MNRAS*, **298**, 525
- Prudil Z., Dékány I., Catelan M., Smolec R., Grebel E. K., Skarka M., 2019, *MNRAS*, **484**, 4833
- Prudil Z., Kunder A., Dékány I., Koch-Hansen A. J., 2024, *A&A*, **684**, A176
- Rich R. M., et al., 1997, *ApJ*, **484**, L25
- Riello M., De Angeli F., Evans D. W., et al. 2021, *A&A*, **649**, A3
- Salaris M., Chieffi A., Straniero O., 1993, *ApJ*, **414**, 580
- Sandage A., Wallerstein G., 1960, *ApJ*, **131**, 598
- Schlegel D. J., Finkbeiner D. P., Davis M., 1998, *ApJ*, **500**, 525
- Schröder K.-P., Cuntz M., 2005, *ApJ*, **630**, L73
- Schroder K.-P., Pols O. R., Eggleton P. P., 1997, *MNRAS*, **285**, 696
- Silva Aguirre V., Catelan M., Weiss A., Valcarce A. A. R., 2008, *A&A*, **489**, 1201
- Soszyński I., et al., 2013, *Acta Astron.*, **63**, 21
- Soszyński I., et al., 2014, *Acta Astron.*, **64**, 177
- Stetson P. B., 2000, *PASP*, **112**, 925
- Tsapras Y., et al., 2017, *MNRAS*, **465**, 2489
- Udalski A., Szymanski M., Kaluzny J., Kubiak M., Mateo M., 1992, *Acta Astron.*, **42**, 253
- VandenBerg D. A., Bergbusch P. A., Ferguson J. W., Edvardsson B., 2014, *ApJ*, **794**, 72
- VandenBerg D. A., Durrell P. R., 1990, *AJ*, **99**, 221
- Vasiliev E., Baumgardt H., 2021, *MNRAS*, **505**, 5978
- Yepez M. A., Arellano Ferro A., Deras D., 2020, *MNRAS*, **494**, 3212
- Yepez M. A., Arellano Ferro A., Deras D., Bustos Fierro I., Muneer S., Schröder K. P., 2022, *MNRAS*,
- Yepez M. A., Arellano Ferro A., Bustos Fierro I., Luna A., 2023, *MNRAS*, **524**, 1503
- Zhang T., Ramakrishnan R., Livny M., 1996, *SIGMOD Rec.*, **25**, 103
- Zinn R., West M. J., 1984, *ApJS*, **55**, 45

APPENDIX A: VARIABLES IN THE FIELD OF NGC6558

In Table A1 the variables found in the field of the cluster are listed with the cross identification from their sources, i.e. the CVSGC (Clement et al. 2001), OGLE (Soszyński et al. 2013), (Soszyński et al. 2014) and *Gaia*-DR3 (Gaia Collaboration et al. 2018). The

membership status is indicated by an asterisk in column 3. In Table A2 there are reported the intensity weighted mean magnitudes, amplitudes and epochs for all variables in the field, regardless they are members or not.

APPENDIX B: LIGHT CURVES

For all light curves we adopted the same colour code to distinguish from the data source and observing run as follows: green: SWOPE, Blue: BA18, Turquoise; BA19, Black: OGLEIII, Red: OGLEIV, Purple: *Gaia*-DR3. Fig. B3 the light curves of the variables reported by *Gaia*-DR3 are shown. Some stars do not show a clear variability. Clear variations are found in G8 which phases well with a period of 70.985 days, and G10 for which a period of 0.178146 d was found. G8 and G10 were the only stars in this batch found to be variables, however being field stars we refrained from assigning them a 'V' number.

This paper has been typeset from a \TeX/L\AA\TeX file prepared by the author.

Table A1. Crossmatch between OGLE and *Gaia*-DR3 identifications of variable stars in the field of NGC 6558.

ID Star	ID OGLE (OGLE-BLG+)	ID GAIA	ID Star	ID OGLE (OGLE-BLG+)	ID GAIA
V1	RRLYR-14886	4048864059416545280*	O22	ECL-342853	4048864059416638208
V2	—————	4048864432989883264*	O23	ECL-342957	4048864506093328768
V3	RRLYR-14929	4048864265574910592*	O24	ECL-343193	4048863750138723840
V4	RRLYR-14866	4048864025056821888*	O25	ECL-343374	4048860692161846400
V5	RRLYR-14867	4048865257631129856*	O26	ECL-343590	4048863784560136832
V6	RRLYR-14888	4048863814514496384*	O27	ECL-343705	4048860790969550208
V7	—————	4048864403013942528	O28	ECL-343910	4048860825368698624
V8	RRLYR-14897	4048860692161845760	O29	ECL-343918	4048864467349644928
V9	RRLYR-14732	4048841480684585600	O30	ECL-344196	4048864368615454336
V10	—————	4048861306252440832	O31	ECL-344354	4048864192625493120
V11	—————	4048865223264032896	O32	ECL-344375	4048864162495551616
V12	—————	4049052758715416320	O33	ECL-344488	4048861207517918080
V13	RRLYR-14809	4049053308471439744	O34	ECL-344503	4048864604944711296
V14	RRLYR-15057	4048862513227644032	O35	ECL-344522	4048860550488673408
V15	—————	4048841102727354368	O36	ECL-344792	4048860550488742016
V16	RRLYR-14912	4048864226982967168*	O37	ECL-344831	4048864295704788736
V17	RRLYR-14892	4048864055040290176*	O38	ECL-345018	4048861344956949504
V18 (O20)	ECL-342710	4048863711547338752*	O39	ECL-345114	4048861173199302528
V19 (G5)	—————	4048864226831441920*	O40	ECL-345412	4048861173157993600
O1	DSCT-08146	4048864089504042880	O41	ECL-345522	4048861168966369152
O2	DSCT-08222	4048863848986229504	O42	ECL-345774	4048860962807893632
O3	DSCT-14210	4048864746611547008	O43	ECL-346064	4048861306407735424
O4	ECL-340840	4048864780971419776	O44	ELL-021823	4048860829601924480
O5	ECL-341024	4048864707979313408	O45	ELL-021837	4048864196855360640
O6	ECL-341028	4048840488628088320	O46	ELL-021862	4048861168854110720
O7	ECL-341420	4048864918370561280	O47	RRLYR-14873	4048864059416651392
O8	ECL-341506	4048840419908456320	O48	DSCT-08146	—————
O9	ECL-341526	4048863956337442432	O49	ECL-346111	44048866254056274176
O10	ECL-341544	4048864849690854016	O50	RRLYR-14709	—————
O11	ECL-341790	4048863990697244800	O51	DSCT-08190	4048840007591268224
O12	ECL-341801	4048864845419442432	O52	ECL-339704	4048841480795839872
O13	ECL-341917	4048865326382558848	O53	ECL-344368	4048866155360805632
O14	ECL-342132	4048864089504046976	O54	ECL-345391	4048866116773356416
O15	ECL-342151	4048864089504247680	O55	ECL-346668	4048865983561808128
O16	ECL-342461	4048864025017002368	O56	-DSCT-14242	—————
O17	ECL-342462	4048864884050514432	N1	—————	—————
O18	ECL-342540	4048864025056864896	N2	—————	4048866155360747776
O19	ECL-342585	4048863608466744320	G8	—————	4048861173198138752
O21	ECL-342716	4048864025057644416	G10	—————	4048863608355972480

* Cluster member star

Table A2. General data for variables in the field of the cluster. The large majority are not cluster member stars. All periods and epochs were estimated in the present work.

ID	Variable Type	$\langle V \rangle$ (mag)	$\langle I \rangle$ (mag)	A_V (mag)	A_I (mag)	P (days)	Epoch (+245 0000.)	RA (2000.)	DEC (2000.)	m/f/u
V1	RRab	16.634	15.662	1.154	0.854	0.466592	2869.64820	18:10:15.59	-31:45:54.10	m
V2	CST	13.553	11.307	—	—	—	—	18:10:16.26	-31:45:03.46	m
V3	RRab	16.280	15.376	1.285	0.859	0.588021	2574.51730	18:10:21.64	-31:45:15.57	m
V4	RRab	16.439	15.543	1.262	0.899	0.503936	8334.65550	18:10:13.27	-31:46:16.03	m
V5	RRab	16.836	15.610	0.863	0.520	0.748679	5749.55520	18:10:13.48	-31:43:45.12	f
V6	RRc	16.466	15.629	0.572	0.323	0.312489	2563.53700	18:10:15.88	-31:46:41.44	m
V7	CST	14.603	13.632	—	—	—	—	18:10:25.61	-31:43:33.19	f
V8	RRab	16.478	15.505	1.308	0.790	0.574526	2916.61750	18:10:17.87	-31:48:55.31	f
V9	RRab	16.514	15.634	1.322	0.867	0.454453	5453.62460	18:09:50.47	-31:46:37.28	f
V10	L	13.978	11.831	—	—	—	—	18:10:36.26	-31:45:31.36	f
V11	L	15.230	12.791	—	—	—	—	18:10:01.62	-31:42:05.43	f
V12	L	16.037	10.689	—	—	—	—	18:09:53.86	-31:43:25.82	f
V13	RRc	16.431	15.554	0.384	0.283	0.360992	2563.53700	18:10:04.75	-31:40:24.89	f
V14	RRc	16.412	15.496	0.514	0.386	0.265041	2808.87910	18:10:45.76	-31:46:20.29	f
V15	L	15.230	11.944	—	—	—	—	18:09:54.16	-31:48:10.89	f
V16	RRab	16.579	15.413	0.386	0.256	0.687550	2135.69400	18:10:19.63	-31:46:05.97	m
V17	RRab	16.250	15.255	0.229	0.149	0.755803	2432.77310	18:10:16.21	-31:45:42.38	m
V18 (O20)	ECL	19.549	18.130	0.543	0.569	0.406042	7000.39400	18:10:12.50	-31:47:33.78	m
V19 (G5)	SR/L	13.7550	11.527	—	—	346.185375	6911.53619	18:10:17.67	-31:45:39.42	m
N1	RRc	16.573	15.663	0.189	0.188	0.303797	8376.55965	18:10:40.99	-31:39:48.18	—
N2	RRc	16.067	15.311	0.257	0.219	0.342412	8692.56056	18:10:25.66	-31:41:59.10	f
G8	—	17.198	13.655	1.674	0.977	70.985000	8692.54054	18:10:30.45	-31:46:34.60	f
G10	—	15.727	14.752	0.108	0.043	0.178146	8698.51780	18:10:11.80	-31:48:22.30	f
O1	DSCT	17.679	16.887	0.426	0.227	0.072299	7000.06928	18:10:06.54	-31:45:38.03	f
O2	DSCT	17.905	16.589	0.323	0.194	0.105038	7000.01133	18:10:17.53	-31:45:50.60	u
O3	DSCT	17.494	16.610	—	—	0.068512	7000.02705	18:10:03.57	-31:46:07.34	f
O4	ECL	18.056	17.013	0.547	0.380	1.734955	5351.90512	18:09:59.66	-31:45:25.98	f
O5	ECL	16.617	15.776	0.504	0.454	1.018260	7000.91980	18:10:01.10	-31:45:44.82	f
O6	ECL	15.050	14.183	0.173	0.166	0.442419	7000.22190	18:10:01.12	-31:47:15.03	f
O7	ECL	18.284	17.403	0.362	0.411	0.442263	7000.08360	18:10:03.85	-31:44:42.05	f
O8	ECL	17.792	17.017	0.233	0.269	0.426111	7000.00280	18:10:04.34	-31:48:04.62	f
O9	ECL	19.690	18.397	0.302	0.284	0.393296	7000.27860	18:10:04.45	-31:47:15.00	u
O10	ECL	18.543	17.386	0.310	0.324	0.442397	7000.29750	18:10:04.63	-31:44:50.95	f
O11	ECL	20.183	18.857	0.493	0.443	0.380086	7000.32450	18:10:06.24	-31:46:10.00	u
O12	ECL	19.728	18.400	0.372	0.352	0.316283	7000.12300	18:10:06.34	-31:44:48.65	f
O13	ECL	—	19.290	—	0.665	0.349780	7000.02210	18:10:07.02	-31:42:53.30	u
O14	ECL	20.696	19.380	0.521	0.471	0.340083	7000.25920	18:10:08.35	-31:45:49.62	f
O15	ECL	20.059	18.807	0.677	0.691	0.344149	7000.14650	18:10:08.46	-31:45:44.71	u
O16	ECL	20.377	18.956	0.486	0.464	0.332756	7000.29330	18:10:10.76	-31:46:10.60	f
O17	ECL	20.692	19.147	0.439	0.599	0.331755	7000.20540	18:10:10.53	-31:44:25.00	u
O18	ECL	18.459	17.418	0.273	0.321	0.458385	7000.13760	18:10:11.10	-31:46:19.52	f
O19	ECL	19.884	17.033	—	0.696	4.065424	7001.22200	18:10:11.47	-31:48:48.83	f
O21	ECL	18.876	17.581	—	0.349	0.751831	7000.27140	18:10:12.54	-31:45:53.50	f
O22	ECL	18.999	17.379	0.358	0.435	3.808711	7000.09620	18:10:13.26	-31:45:22.93	f
O23	ECL	18.535	17.657	0.166	0.210	0.359152	7000.20550	18:10:14.00	-31:44:19.35	f
O24	ECL	18.753	17.451	0.217	0.193	0.509554	7000.04880	18:10:15.82	-31:47:50.00	f
O25	ECL	19.250	18.133	0.306	0.289	0.365249	7000.23660	18:10:17.06	-31:49:05.86	f
O26	ECL	—	18.955	—	0.574	0.333312	7000.20130	18:10:18.46	-31:46:45.40	u
O27	ECL	18.177	17.238	0.146	0.521	2.618627	7000.27960	18:10:19.40	-31:47:40.97	f
O28	ECL	19.659	18.546	0.206	0.335	0.295708	7000.01300	18:10:20.84	-31:47:18.12	f
O29	ECL	15.784	14.951	0.017	0.039	0.503074	7000.50200	18:10:20.93	-31:44:35.63	f
O30	ECL	20.220	18.930	0.749	0.700	0.373394	7000.02310	18:10:22.80	-31:44:23.90	u
O31	ECL	19.239	17.887	0.244	0.313	1.363473	7001.22150	18:10:23.91	-31:45:43.19	f
O32	ECL	14.242	13.470	0.404	0.402	0.535965	7000.22590	18:10:24.09	-31:46:08.91	f
O33	ECL	18.992	18.075	0.291	0.317	0.580938	7000.44860	18:10:24.95	-31:47:08.20	f
O34	ECL	20.253	18.315	—	0.524	1.720336	7001.19860	18:10:25.11	-31:43:12.64	f
O35	ECL	19.605	18.351	0.654	0.639	6.403002	7003.56750	18:10:25.25	-31:48:51.00	f
O36	ECL	20.372	18.979	0.770	0.521	0.290533	7000.19830	18:10:27.16	-31:49:02.40	u
O37	ECL	17.569	16.589	0.786	0.911	1.613186	7000.58810	18:10:27.48	-31:44:53.58	f
O38	ECL	19.260	17.887	0.142	0.187	0.319237	7000.31290	18:10:28.62	-31:45:40.46	f
O39	ECL	20.669	19.249	0.806	0.694	0.246369	7000.22250	18:10:29.30	-31:46:55.10	u
O40	ECL	17.635	16.641	0.307	0.331	0.519652	7000.00290	18:10:31.42	-31:47:02.82	f

Table A2. Continue

ID	Variable Type	$\langle V \rangle$ (mag)	$\langle I \rangle$ (mag)	A_V (mag)	A_I (mag)	P (days)	Epoch (+245 0000.)	RA (2000.)	DEC (2000.)	m/f/u
O41	ECL	20.372	18.486	0.620	0.541	0.454164	7000.10650	18:10:32.03	-31:47:07.00	f
O42	ECL	18.879	17.705	0.243	0.292	0.429635	7000.23460	18:10:33.81	-31:47:53.74	f
O43	ECL	18.270	17.183	0.139	0.163	0.620570	7000.37790	18:10:35.68	-31:45:26.14	f
O44	ECL	16.899	15.401	0.081	0.085	12.114004	7001.22140	18:10:22.82	-31:47:55.70	f
O45	ECL	14.563	13.903	0.044	0.050	0.635088	7000.24380	18:10:24.56	-31:45:17.47	f
O46	ECL	19.146	17.875	0.147	0.177	0.349893	7000.22270	18:10:29.17	-31:46:54.22	f
O47	RRL	16.731	15.526	0.357	0.250	0.672365	7000.26497	18:10:14.22	-31:45:08.23	f
O48	DSCT	17.667	16.833	0.523	0.289	0.086767	8296.85025	18:09:48.88	-31:53:21.90	—
O49	ECL	16.333	15.444	0.530	0.492	0.488999	7000.27340	18:10:35.97	-31:40:13.90	f
O50	RRLYR	15.745	14.778	0.490	0.387	0.359998	8376.60649	18:09:44.80	-31:52:29.00	—
O51	DSCT	17.114	16.292	0.446	0.270	0.121344	8334.66273	18:10:04.98	-31:51:12.20	f
O52	ECL	18.427	17.279	0.498	0.500	0.436376	7000.36760	18:09:52.27	-31:46:30.40	f
O53	ECL	18.222	17.084	0.351	0.374	0.491644	7000.02930	18:10:24.06	-31:41:41.50	u
O54	ECL	17.884	17.049	0.326	0.264	0.535841	7000.09500	18:10:31.23	-31:41:26.90	f
O55	ECL	18.004	16.996	0.442	0.299	0.681172	8296.73116	18:10:39.61	-31:41:21.80	f
O56	DSCT	17.892	16.919	—	—	0.065044	8296.63391	18:09:44.80	-31:52:29.00	—

* m- cluster member, f- field star, u- unknown due to lack of proper motion

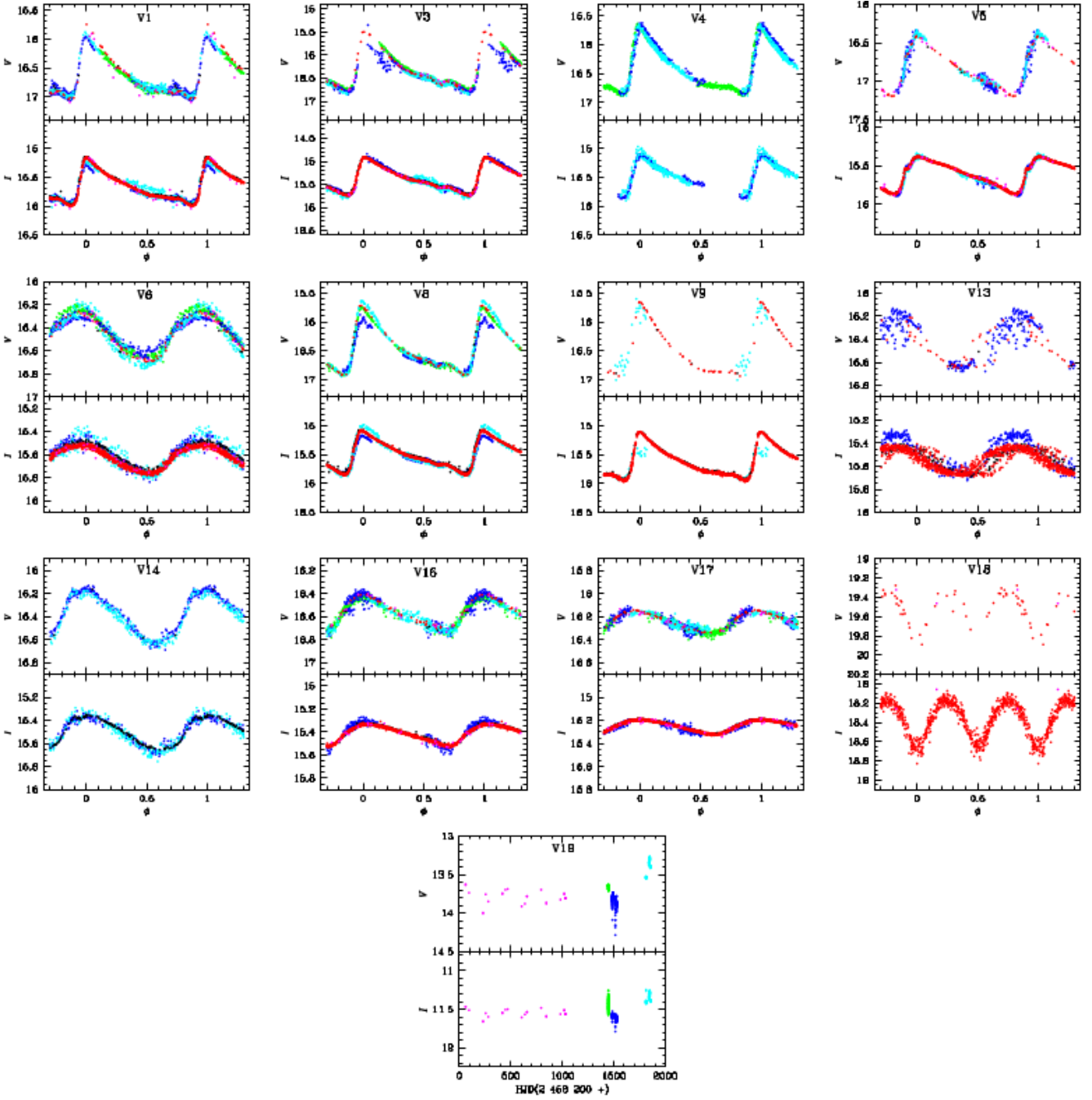


Figure B1. Light curves of variables reported the CVSGC (Clement et al. 2001) (2016 edition), plus the two new cluster member variables noticed in this work, V18 and V19. Except for V4, where a Blazhko modulation of 26.73 days was found (see section 6), we have not detected secondary frequencies among the scattered light curves. In all cases the scatter is intrinsic to the photometric uncertainties.

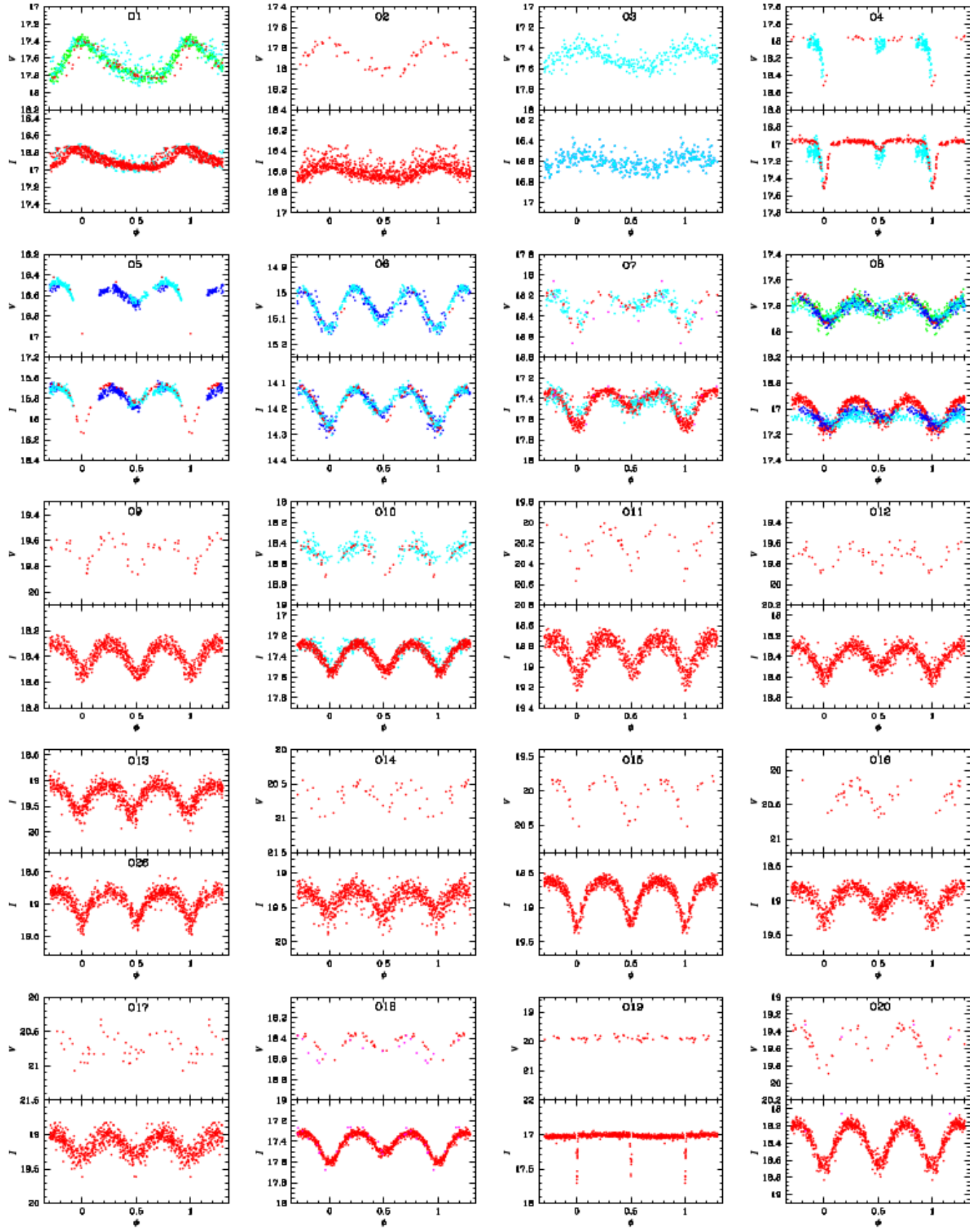


Figure B2. Light curves of the 56 variables identified in the OGLE database. A period modulation cannot be ruled out in O50 but our data are insufficient to quantify it.

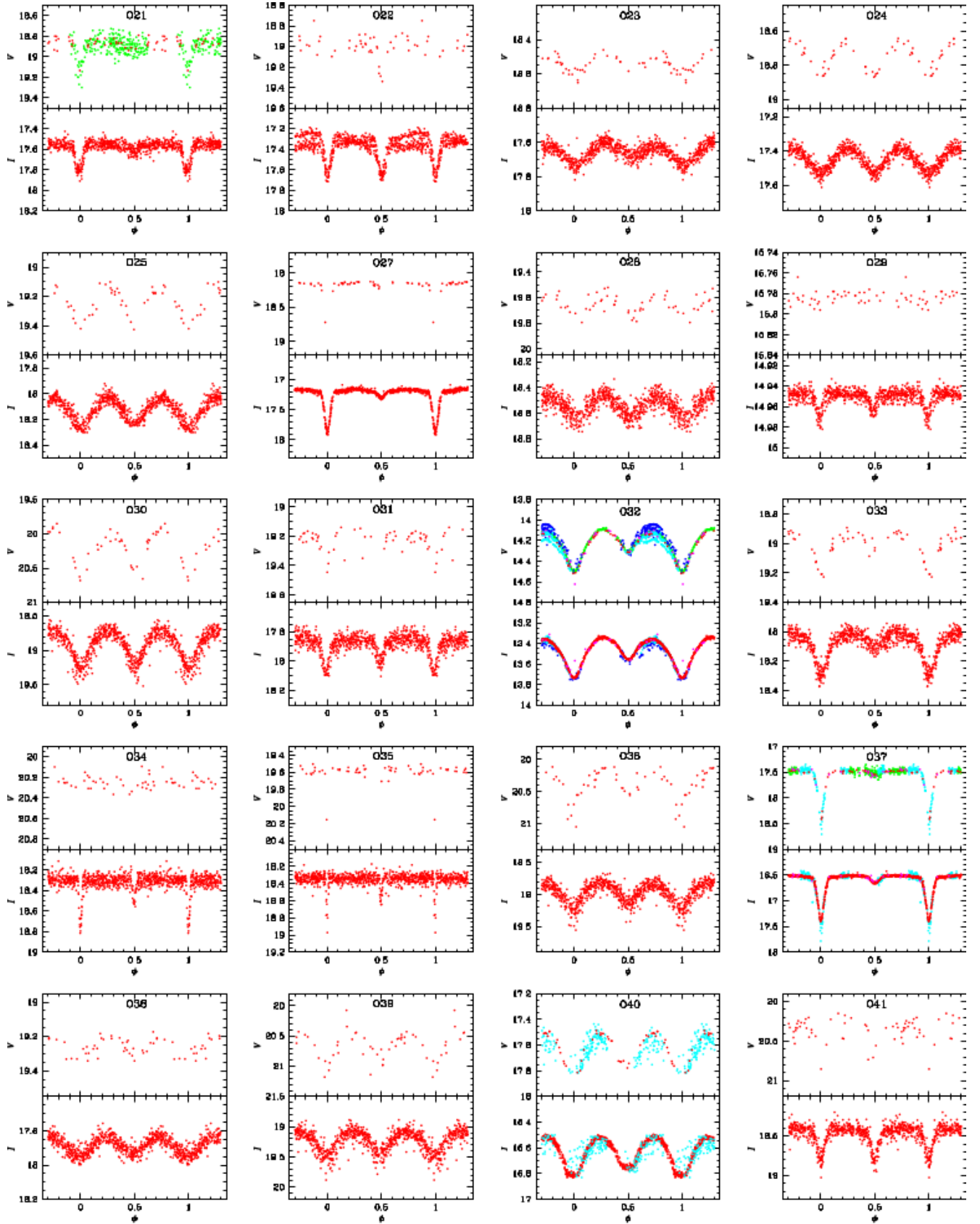


Figure B2. Continued

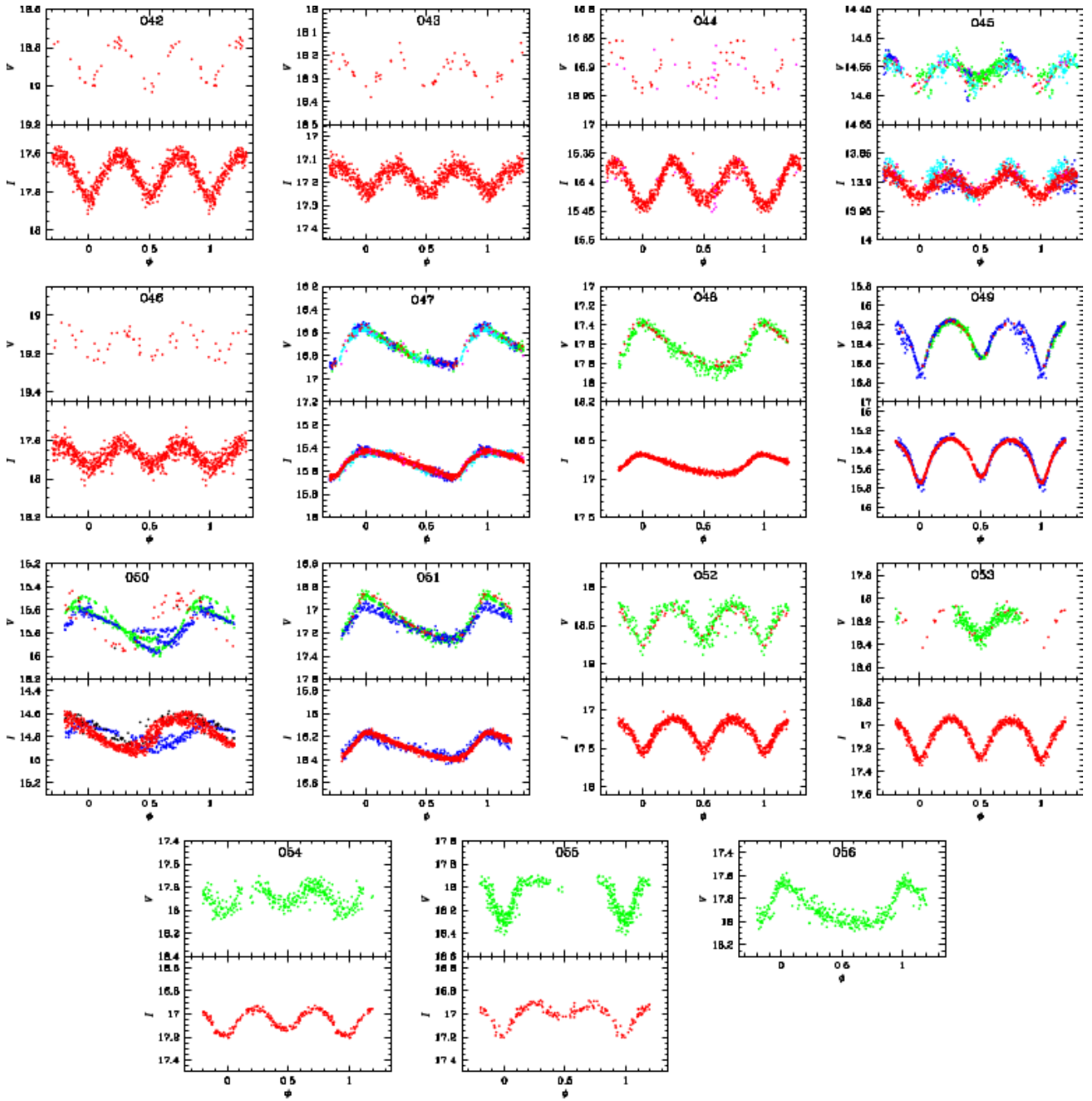
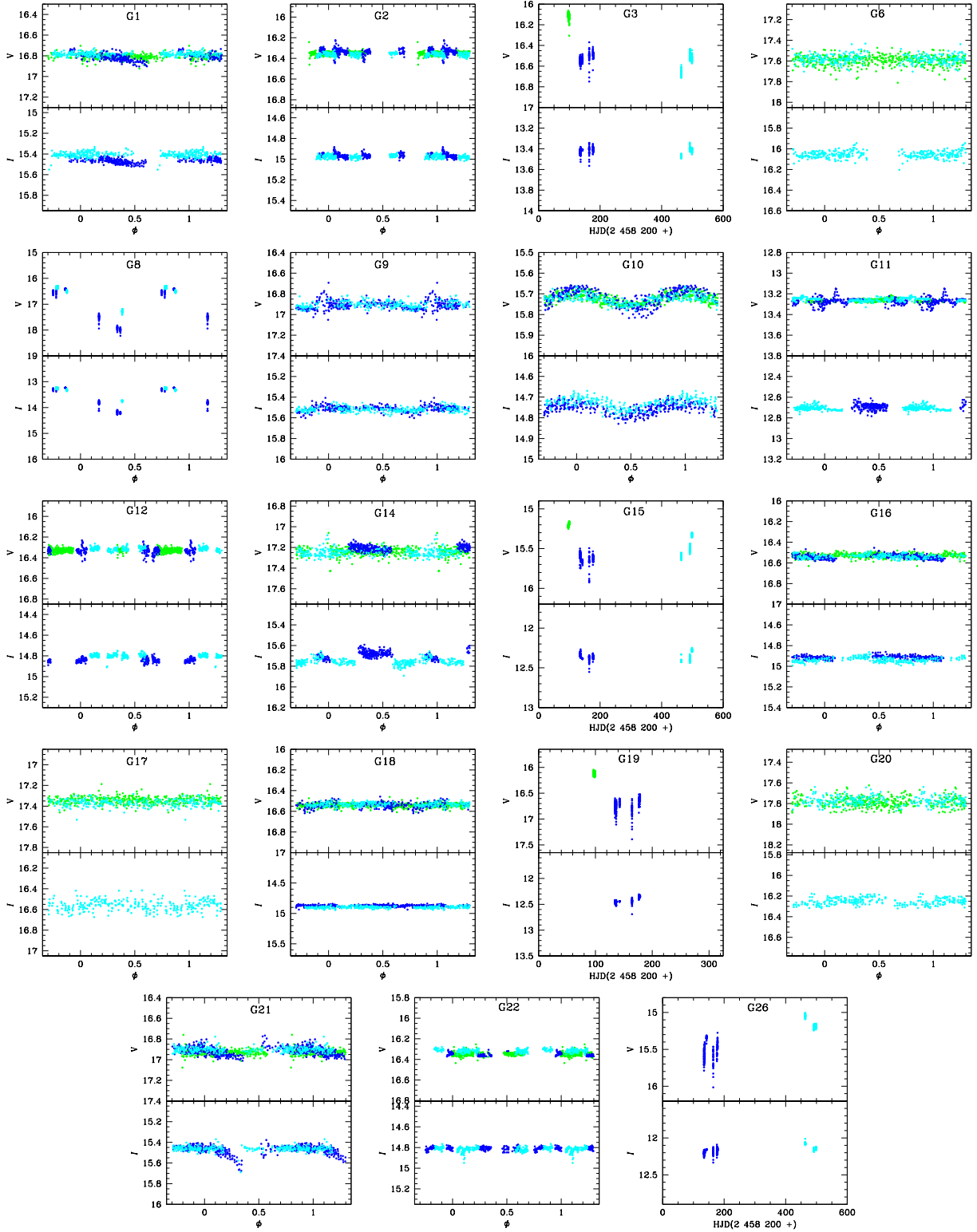


Figure B2. Continue.



1

Figure B3. Light curves of variables reported in *Gaia*-DR3. Although long-period variability cannot be ruled out when plotted vs HJD in stars G3, G15, G19 and G26, further data would be required to establish them as true variables. Clear variations are found in G8 which phases nicely with a period of 70.985 days, and G10 for which a period of 0.178146 d was found. However, from their proper motion analysis they seem to be field stars.